ANNUAL REVIEWS

Annual Review of Earth and Planetary Sciences

Bubble Formation in Magma

James E. Gardner,[1] Fabian B. Wadsworth,[2] Tamara L. Carley,[3] Edward W. Llewellin,[2] Halim Kusumaatmaja,[4] and Dork Sahagian[5]

[1]Jackson School of Geosciences, University of Texas at Austin, Austin, Texas, USA; email: gardner@jsg.utexas.edu

[2]Department of Earth Sciences, Durham University, Durham, United Kingdom

[3]Department of Geology and Environmental Geosciences, Lafayette College, Easton, Pennsylvania, USA

[4]Department of Physics, Durham University, Durham, United Kingdom

[5]Department of Earth and Environmental Sciences, Lehigh University, Bethlehem, Pennsylvania, USA

Annu. Rev. Earth Planet. Sci. 2023. 51:131–54

First published as a Review in Advance on November 28, 2022

The *Annual Review of Earth and Planetary Sciences* is online at earth.annualreviews.org

https://doi.org/10.1146/annurev-earth-031621-080308

Keywords

nucleation, volcanic eruption, magma, spinodal decomposition, bubble dynamics, volatiles

Abstract

Volcanic eruptions are driven by bubbles that form when volatile species exsolve from magma. The conditions under which bubbles form depend mainly on magma composition, volatile concentration, presence of crystals, and magma decompression rate. These are all predicated on the mechanism by which volatiles exsolve from the melt to form bubbles. We critically review the known or inferred mechanisms of bubble formation in magmas: homogeneous nucleation, heterogeneous nucleation on crystal surfaces, and spontaneous phase separation (spinodal decomposition). We propose a general approach for calculating bubble nucleation rates as the sum of the contributions from homogeneous and heterogeneous nucleation, suggesting that nucleation may not be limited to a single mechanism prior to eruption. We identify three major challenges in which further experimental, analytical, and theoretical work is required to permit the development of a general model for bubble formation under natural eruption conditions.

- We review the mechanisms of bubble formation in magma and summarize the conditions under which the various mechanisms are understood to operate.

- Bubble formation mechanisms may evolve throughout magma ascent as conditions change such that bubbles may form simultaneously and sequentially via more than one mechanism.
- Contributions from both homogeneous nucleation and heterogeneous nucleation on multiphase crystal phases can be captured via a single equation.
- Future work should focus on constraining macroscopic surface tension, characterizing the microphysics, and developing a general framework for modeling bubble formation, via all mechanisms, over natural magma ascent pathways.

1. INTRODUCTION

Magma at depth contains dissolved volatile species that form bubbles when they come out of solution (Sparks 1978; Proussevitch & Sahagian 1996, 1998, 2005; Sahagian 2005; Girona et al. 2016; Tramontano et al. 2017). Bubbles typically form and grow in response to decompression during magma ascent, which is itself a result of the buoyancy introduced to the system by the formation of a free gas phase (Blake 1984, Tait et al. 1989). Eruption style depends fundamentally on bubble growth processes. Fragmentation of magma, which is the defining characteristic of explosive volcanic eruptions, is driven by the pressure within growing gas bubbles. This, in turn, depends on the depth and rate of bubble formation and the spatial density of bubbles (i.e., bubble number density) (Sahagian 1999). These characteristics are controlled by the bubble formation process.

The formation of gas bubbles within magma occurs at depth, so it cannot be directly observed, leaving us to infer the mechanism of gas bubble formation from theory, experimentation, and observations of natural eruptive products (e.g., ash, pumice, vesicular lava). Existing experimental evidence suggests that volatiles exsolve via bubble nucleation or spontaneous phase separation (e.g., Hurwitz & Navon 1994, Gardner & Denis 2004, Allabar & Nowak 2018).

The earliest experimental studies in this area focused on bubble nucleation both homogeneously from silicate melt and heterogeneously on crystal surfaces (Hurwitz & Navon 1994). Subsequent studies have investigated the influences of melt and volatile compositions, changes in intensive parameters (pressure, temperature), and the occurrence of seed nucleation sites (e.g., Mourtada-Bonnefoi & Laporte 1999, 2002, 2004; Mangan & Sisson 2000, 2005; Gardner & Denis 2004; Mangan et al. 2004; Gardner 2007, 2012; Iacono-Marziano et al. 2007; Cluzel et al. 2008; Larsen 2008; Hamada et al. 2010; Cichy et al. 2011; Gardner & Ketcham 2011; Gondé et al. 2011; Gardner et al. 2013, 2018; Gonnermann & Gardner 2013; Hardiagon et al. 2013; Fiege et al. 2014; Gardner & Webster 2016; Le Gall & Pichavant 2016b; Preuss et al. 2016; Hajimirza et al. 2019, 2021a,b). Despite numerous and rigorous experimental studies, much remains to be learned about the mechanics of gas phase formation within magmas.

The aims of this review are to both provide background on what is currently known about the formation of gas bubbles in silicate melts and spur future studies to answer vexing questions that remain. We first summarize the driving mechanism for gas phase separation in magmas and the basic mechanics of gas bubble formation. We then propose three grand challenges aimed at closing existing knowledge gaps on bubble formation in magmas related to constraining surface tension for silicate melts, constraining the microphysics of nucleation on heterogeneities, and interpreting bubble formation histories from natural eruptive products. By overcoming these knowledge gaps, the volcanological community will be able to formulate a more complete model for gas phase separation, allowing us to better infer eruptive mechanisms and degassing at depth.

1.1. The Driving Mechanism for Gas Exsolution from Magmas

Bubbles form in magmas when volatile elements become supersaturated in the silicate melt (Sparks 1978). The most abundant volatile in magmas is H_2O; in the case of mafic magmas, CO_2 is commonly also abundant (Johnson et al. 1994). The solubilities of both H_2O and CO_2 are controlled by vapor pressure (e.g., Fogel & Rutherford 1990, Blank et al. 1993, Tamic et al. 2001, Newman & Lowenstern 2002, Papale et al. 2006, Ghiorso & Gualda 2015), melt composition (e.g., Moore et al. 1998, Dixon 1997, Di Matteo et al. 2004, Lesne et al. 2011, Romano et al. 2021), and temperature (e.g., Holtz et al. 1995). Extensive experimental work has led to well-calibrated models that predict the solubilities of H_2O and CO_2 as functions of melt and fluid compositions, pressure, and temperature, for either specific melt compositions (e.g., Dixon et al. 1995, Newman & Lowenstern 2002, Di Matteo et al. 2004, Liu et al. 2005, Ryan et al. 2015, Schanofski et al. 2019) or more generalized magmatic systems (e.g., Papale et al. 2006, Iacono-Marziano et al. 2012, Ghiorso & Gualda 2015, Allison et al. 2022).

Most experimental work has focused on the formation of H_2O bubbles in silicate melts because H_2O is the most abundant volatile and because the H_2O content in a silicate melt has a dramatic impact on melt viscosity (Hess & Dingwell 1996), diffusivities of other chemical species (e.g., Freda et al. 2005, Alletti et al. 2007), and the crystallization rates in the magma (e.g., Hammer & Rutherford 2002, Couch et al. 2003, Applegarth et al. 2013). The high solubility of H_2O causes it to saturate and form bubbles at relatively shallow depths. CO_2 is far less soluble in silicate melts, which means that the formation of CO_2 bubbles likely occurs at greater depths than H_2O bubbles (e.g., Pichavent et al. 2013, Le Gall & Pichavant 2016b). Bubble formation from experimental systems with mixed fluids ($H_2O + CO_2$) has found differing results. Le Gall & Pichavant (2016b) found that the presence of CO_2 in basaltic melt led to multiple nucleation events during decompression. In contrast, CO_2 in H_2O-rich rhyolitic melts does not appear to enhance bubble nucleation (Gardner & Webster 2016).

The solubilities of other volatile species such as SO_2, H_2S, HCl, and HF are limited by saturation with a solid or immiscible liquid phase (e.g., Luhr 1990, Carroll & Webster 1994, Webster et al. 1999, Jugo et al. 2005, Moune et al. 2009). No experimental study has focused on bubble nucleation driven by supersaturation of these volatiles. Fluorine, however, has been found to significantly enhance the nucleation of H_2O bubbles in rhyolitic melt relative to F-poor melts (Gardner et al. 2018).

2. BUBBLE NUCLEATION MECHANISMS AND RATES

When a volatile species becomes supersaturated in silicate melt, molecules of that volatile can cluster together in response to thermal, chemical, or physical perturbations (**Figure 1**). As volatiles cluster together into a new phase, the overall free energy of the system is reduced, and a greater reduction occurs with larger clusters (i.e., more volatile species clustered together) (Hirth et al. 1970, Hurwitz & Navon 1994). But when volatiles and silicate melt separate into two phases, an interface is created, which contributes an increase in the free energy, collectively resulting in a macroscopic surface tension, σ_∞. (Note that **Table 1** collates notation and definitions of variables used in this work.) Here, σ_∞ is the surface tension of a fully developed interface equivalent to the macroscopically measurable interfacial tension between the magmatic vapor phase and the melt phase, where the subscript ∞ denotes an interface of large radius of curvature. Because larger clusters have greater surface areas, the gain in energy increases as clusters grow larger. A competition arises between the reduction in free energy resulting from forming a new volatile phase and the increase in free energy caused by forming a new surface. This is a trade-off that changes as bubbles get larger because the reduction of energy with volume outpaces the gain from increased surface

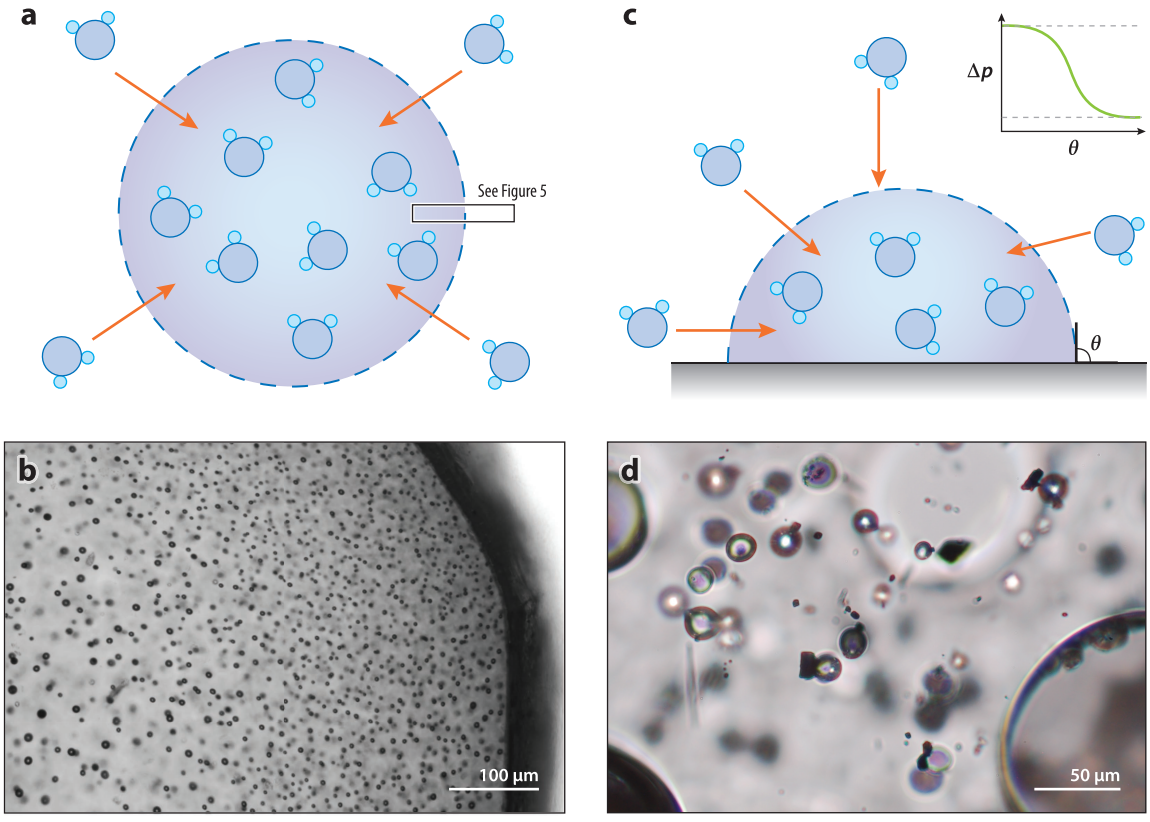

Figure 1

Mechanisms for bubble nucleation in silicate melts. (*a*) Homogeneous nucleation involves volatiles clustering together to form a new phase in an otherwise homogeneous medium (in this case, silicate melt). The small rectangle shows the region of interest discussed in **Figure 5**. (*b*) H_2O bubbles nucleated homogeneously in high-silica rhyolitic melt. (*c*) Heterogeneous nucleation involves volatiles clustering together to form a new phase on a surface (in this case, a crystal), with the supersaturation needed for nucleation depending on the contact angle (θ) between the bubble and surface. (*d*) H_2O bubbles nucleated on magnetite crystals (*opaque rectangles* and *squares*) in high-silica rhyolitic melt.

area. There thus exists a critical cluster size, r_c, at which the sum of the changes in free energy, expressed as a function of cluster radius, reaches a maximum (Hirth et al. 1970, Hurwitz & Navon 1994). For clusters smaller than r_c, the increase in surface energy exceeds the energy reduction from decreased supersaturation. The addition of another volatile molecule into the cluster thus leads to an overall increase in free energy, and so the cluster (called an embryo) is not viable and will dissipate. If, however, a cluster exceeds r_c, then the addition of new molecules reduces the system energy and hence the cluster is energetically favorable and considered a viable nucleus.

Volatiles cluster together either homogeneously within the melt or heterogeneously on crystal surfaces (**Figure 1**). The essential difference between homogeneous and heterogeneous nucleation is the effective total surface energy, which is greatest for homogeneous nucleation in the absence of wettable crystal surfaces.

2.1. Homogeneous Nucleation

The rate of formation of critically sized clusters in classical nucleation theory is based on an assumed steady state (e.g., Hirth et al. 1970, Hurwitz & Navon 1994, Debenedetti 1996,

Table 1 Notations used in the text

Term	Definition
a_o	Distance between volatile species
c	Crystal
D	Diffusivity of the volatile in the melt phase
g	$\sqrt{1+\chi^2+2\cos\theta\chi}$
i	Given crystal phase
J	Nucleation rate
J_0	Maximum nucleation rate possible
J_{het}	Nucleation rate, heterogeneous nucleation
J_{hom}	Nucleation rate, homogeneous nucleation
J_i	Nucleation rate for a given phase
J_T	General form for nucleation rate; summation of rates of homogeneous and heterogeneous nucleation
k_B	Boltzmann constant; 1.38×10^{-23} J·K^{-1}
m	Melt
N_B	Vesicle (bubble) number densities
n_o	Number of volatile species per unit volume
p	Ambient pressure of the melt phase
p_b	Internal pressure of the critical nucleus
p_{sat}	Saturation pressure of the melt
R	Crystal radius of curvature
r_c	Critical cluster size
r_e	Equimolecular distance between phases
r_s	Radius of a nucleus
T	Absolute temperature
t	Time
v	Bubble
W_{cl}	Classical work of nucleus formation
Z	Zel'dovich factor
α	Accounts for the deviation from homogeneous nucleation in the presence of surfaces with a given gas–solid wettability; accounts for heterogeneous nucleation rates
α_i	Deviation from homogeneous nucleation for a given phase
β	Dimensionless parameter to account for the number density of nucleation sites
β_i	A scaling factor that allows the number density of crystals to be incorporated into the J_{het} rate
Γ_1	Fugacity coefficient of the volatile phase at the specified pressure and temperature, dependent on p_b and T
Γ_2	Fugacity coefficient of the volatile phase at the specified pressure and temperature, dependent on p_{sat} and T
Δp_c	Supersaturation required for heterogeneous nucleation
Δp_m	Supersaturation required for homogeneous nucleation
Δp	Supersaturation pressure; $p_b - p$
δ_T	Tolman length
θ	Contact angle between the bubble and crystal; balance of surface tension
λ	Wavelength
λ_c	Critical wavelength for water concentration perturbation in spinodal decomposition

(*Continued*)

Table 1 (*Continued*)

Term	Definition
σ_∞	Surface tension of a fully developed interface of large radius of curvature
σ_{ij}	Surface tension between two of the phases: crystal (c), bubble (v), or melt (m)
σ_{nuc}	Surface tension for the nucleus; equimolecular surface as defined by δ_Γ
Ω_L	Molecular volume of H_2O
χ	Ratio between the crystal radius of curvature and the critical nucleus size; R/r_c
ω	Frequency of formation of nuclei > r_c
∞	Interface of large radius of curvature

Mourtada-Bonnefoi & Laporte 2002), as obtained from the dimensionless Zel'dovich factor, Z, which gives the probability that a nucleus at the top of the energy barrier will go on to form the new phase rather than dissolve, such that (Gonnermann & Gardner 2013)

$$Z = \frac{\Omega_L (p_b - p)^2}{8\pi\sigma_\infty^{3/2}\sqrt{k_B T}}, \quad 1.$$

and the frequency ω of formation of nuclei larger than r_c, given by

$$\omega = \frac{16\pi\sigma_\infty^2 n_o D}{a_o (p_b - p)^2}, \quad 2.$$

where Ω_L is the molecular volume of H_2O, k_B is the Boltzmann constant ($k_B = 1.38 \times 10^{-23}$ J·K^{-1}), and T is absolute temperature. The concentration of molecules available for clustering is given by n_o, the number of volatile species per unit volume, and a_o, the distance between them. If volatiles are distributed uniformly, a_o is approximated by $a_o = n_o^{-1/3}$. The driving force for clustering is related to the supersaturation pressure, Δp, which is the difference between the internal pressure of the critical nucleus, p_b, and the ambient pressure of the melt phase, p (i.e., $\Delta p = p_b - p$). In general, p_b will be less than saturation pressure of the melt, p_{sat}, and can be calculated from (Debenedetti 1996, Cluzel et al. 2008)

$$p_b = \Gamma_2 p_{sat} \exp\left(\frac{\Omega (p - p_{sat})}{k_B T}\right) \Gamma_1^{-1}, \quad 3.$$

where Γ_1 and Γ_2 are the fugacity coefficients of the volatile phase at the specified pressure and temperature, in which Γ_1 depends on p_b and T and Γ_2 depends on p_{sat} and T.

Based on classical nucleation theory, the nucleation rate can be written as (Hirth et al. 1970, Hurwitz & Navon 1994, Mourtada-Bonnefoi & Laporte 2002, Gonnermann & Gardner 2013)

$$J = J_0 \exp\left(\frac{-W_{cl}}{k_B T}\right), \quad 4.$$

in which W_{cl} is the classical work of nucleus formation (Gibbs 1961) and is given by

$$W_{cl} = \frac{16\pi\sigma_\infty^3}{3(\Delta p)^2}, \quad 5.$$

and the pre-exponential parameter, J_0, can be written as

$$J_0 = \frac{2\Omega_L n_o^2 D}{a_o}\sqrt{\frac{\sigma_\infty}{k_B T}}, \quad 6.$$

where D is the diffusivity of the volatile in the melt phase. As schematically illustrated in **Figure 2**, J increases rapidly as pressure drops below p_{sat} (i.e., as Δp increases). The value of Δp at which J becomes significant depends on the value of σ_∞. Because J_0 defines the maximum nucleation rate

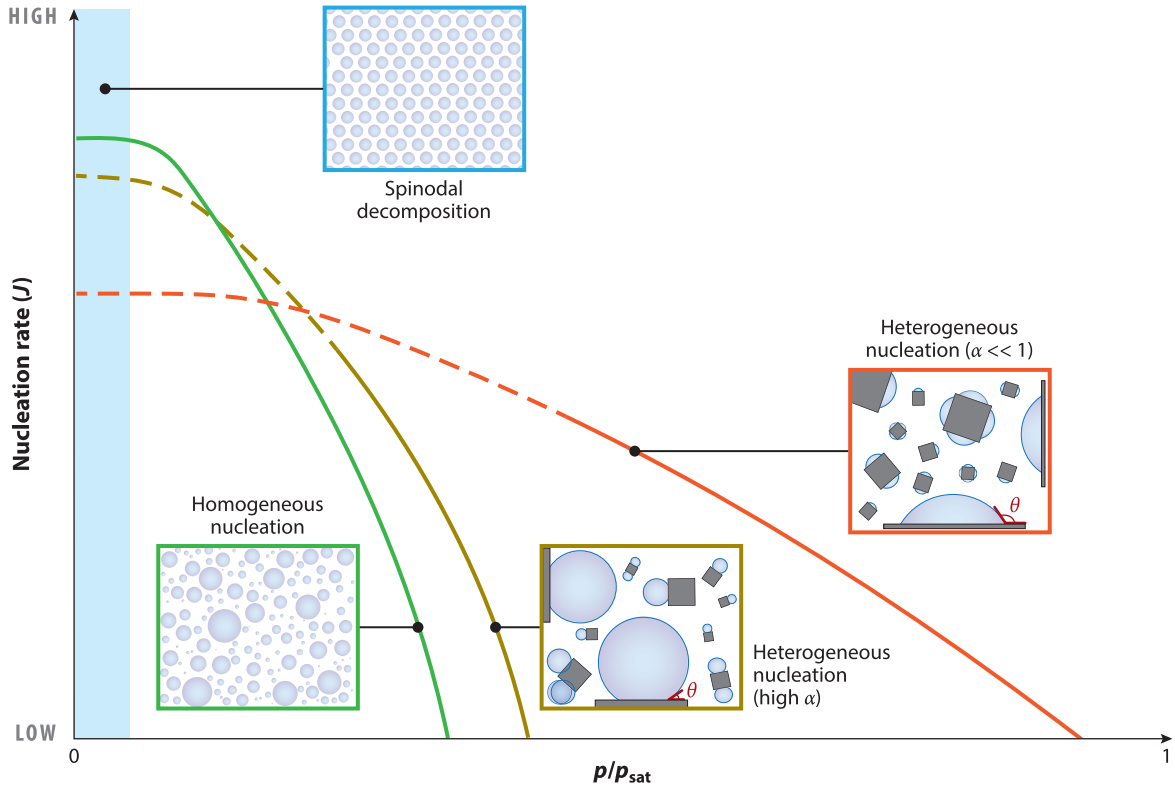

Figure 2

Bubble nucleation rates as a function of H_2O supersaturation in silicate melt. Supersaturation is characterized by p/p_{sat}. Nucleation rate (J) is negligible for all mechanisms at saturation ($p = p_{sat}$). At relatively high supersaturation, the rate of homogeneous nucleation becomes significant, depending on the value of surface tension between H_2O bubbles and silicate melt. The rate of heterogeneous nucleation is significant at relatively lower supersaturations, depending on the wettability of the heterogeneity, which is characterized by α (Equation 8); as α becomes high (and approaches 1), the heterogeneity does not serve as an efficient nucleation site. At high supersaturations, nucleation rate curves asymptote to the pre-exponential term J_o (Equations 4 or 7). For heterogeneous nucleation the rate curves are dashed because that value may differ depending on which crystal phase is involved (i.e., J_i in Equation 11). At extreme supersaturations spinodal decomposition may occur, with bubbles forming simultaneously throughout the magma as a deterministic rather than stochastic process.

possible given by high Δp (i.e., $W_{cl} \rightarrow 0$), J asymptotically approaches J_0 at high supersaturations (**Figure 2**).

For most magmatic models or experimental scenarios, p can be measured or computed, and p_b can be found from Equation 3. Thus W_{cl} depends on σ_∞ as the single unknown. Sparks (1978) argued that Δp must be high to nucleate H_2O bubbles in silicate melts, based on the value for σ_∞ reported in Epel'baum (1973) for hydrous granitic melt. Hurwitz & Navon (1994) experimentally confirmed that Δp must exceed ~60–100 MPa before bubbles nucleate homogeneously in rhyolite melt. Similarly high Δp values have been found in numerous other experimental studies for a range of silicate melt compositions with differing H_2O contents (Mourtada-Bonnefoi & Laporte 1999, 2002, 2004; Mangan & Sisson 2000, 2005; Mangan et al. 2004; Iacono-Marziano et al. 2007; Cluzel et al. 2008; Hamada et al. 2010; Gardner & Ketcham 2011; Gondé et al. 2011; Gardner et al. 2013; Gonnermann & Gardner 2013; Fiege et al. 2014; Le Gall & Pichavant 2016b; Preuss et al. 2016; Hajimirza et al. 2019, 2021a,b).

2.2. Heterogeneous Nucleation

The presence of preexisting surfaces in a magma (e.g., crystals) can provide energetically favorable sites on which volatiles can cluster, thereby lowering the supersaturation needed for bubble nucleation (**Figure 1*c*,*d***). Such sites increase the frequency of formation of viable nuclei by lowering the total energy increase associated with the formation of new interfaces, thus reducing the critical size of bubble nuclei. Classical nucleation theory is usually modified for heterogeneities by introducing a term, α, that accounts for the deviation from homogeneous nucleation in the presence of surfaces with a given gas–solid wettability, such that

$$J = J_0 \exp\left(\frac{-W_{\mathrm{cl}}}{k_B T}\alpha\right), \qquad 7.$$

where α can vary between 1 and 0, with $\alpha = 1$ representing homogeneous nucleation (i.e., no modification) and $\alpha < 1$ representing nucleation on heterogeneities (**Figure 2**). In general, α is a geometric term that modifies the exponential term to account for the balance of surface tensions between the three phases: crystal (c), bubble (v), and melt (m) (Hurwitz & Navon 1994). Assuming that a spherical bubble partially wets a flat surface, α is given as

$$\alpha = \frac{(2 - \cos\theta)(1 + \cos\theta)^2}{4}, \qquad 8.$$

in which θ is the contact angle between the bubble and crystal (**Figure 1*c***) and reflects the balance of surface tensions

$$\cos\theta = \frac{(\sigma_{\mathrm{cv}} - \sigma_{\mathrm{cm}})}{\sigma_{\mathrm{mv}}}, \qquad 9.$$

where σ_{ij} is surface tension between two of the three phases (Landau & Lifshitz 1980, Hurwitz & Navon 1994, Kashchiev 2000). It is evident from consideration of Equations 8 and 9 that heterogeneous nucleation is enhanced most by the presence of crystal phases with a high contact angle (i.e., for which the vapor phase preferentially wets the crystal surfaces) (**Figure 2**).

Hurwitz & Navon (1994) first demonstrated the dramatic impact of crystals in reducing the Δp required to nucleate H_2O bubbles in rhyolitic melts. They found that magnetite reduced Δp from $\gtrsim$60 MPa to as little as ~1 MPa. Zircon and biotite crystals reduced Δp to 30–50 MPa and $\Delta p \geq 30$ MPa, respectively (Hurwitz & Navon 1994). In each of these cases, therefore, $\alpha < 1$. In contrast, bubbles did not appear to wet plagioclase or quartz (i.e., $\theta = 0$), and as such $\alpha = 1$. Since that study, the efficiency of bubble nucleation on other crystal phases, and in diverse melt compositions, has been investigated experimentally with differing results. Gardner & Denis (2004) confirmed that, in rhyolite melts, magnetite enhances nucleation very effectively, hematite is only moderately effective, and plagioclase does not enhance nucleation. Pyroxene has been found to have a small impact on bubble nucleation in phonolitic melt but readily seeded bubbles in andesitic melts (Larsen 2008, Pleše et al. 2018). Plagioclase also enhanced H_2O bubble nucleation in andesitic melts (Pleše et al. 2018), counter to observations made in rhyolitic melts. In fact, silicate minerals are more efficient at seeding nucleation in andesitic melts than are Fe-Ti oxides, whereas the opposite occurs in rhyolitic melts (Hurwitz & Navon 1994, Gardner & Denis 2004, Pleše et al. 2018). For rhyolites, magnetite crystals have been invoked as a primary site for heterogeneous nucleation because magnetite reduces α substantially (Shea 2017, Hajimirza et al. 2021b). The results from bubble nucleation in andesitic melts (Pleše et al. 2018), however, raise the possibility that other phases play a dominant role in heterogeneous bubble nucleation in non-rhyolitic melts. Overall, the significantly reduced supersaturations required for heterogeneous nucleation suggest that it may be the dominant mechanism of bubble formation in natural magmas (Shea 2017, Hajimirza et al. 2021b).

The reduced values of Δp in heterogeneous nucleation result from the bubble nucleus partially wetting the surface of the crystal (Equation 9). It is currently not possible to measure θ for the bubble nucleus–crystal surface interface because of the extremely small size of the nucleus, thought to be only a few nanometers (Navon & Lyakhovsky 1998). Any measurement of contact angle between crystal and macroscopic bubbles has proved inconclusive because of substantial bubble growth following nucleation (Gardner & Denis 2004, Pleše et al. 2018). Instead, contact angles have been approximated from the reduction in Δp needed for nucleation relative to that required in the absence of the crystal surface (Gardner & Denis 2004, Hajimirza et al. 2021b), such that

$$\alpha \approx \frac{\Delta p_c}{\Delta p_m}, \qquad 10.$$

where Δp_c is the supersaturation required for heterogeneous nucleation and Δp_m is the supersaturation required for homogeneous nucleation (**Figure 1*c***). Estimates for α for rhyolitic melts indicate that the contact angle for feldspar is ~0–20°, for pyroxene it is 40–60°, for hematite it is ~90–100°, and for magnetite it is ~145–160° (Hajimirza et al. 2021b).

2.3. Mixed and Evolving Nucleation in Magmas

Modeling studies have attempted to replicate the number density of bubbles (vesicles) and their sizes preserved in natural eruptive products. Models typically restrict nucleation to a single mechanism (e.g., Toramaru 1989, 2006, 2014; Massol & Koyaguchi 2005; Hamada et al. 2010; Le Gall & Pichavant 2016a), which leads to discussions of whether one nucleation dominates over the others (e.g., Shea 2017, Hajimirza et al. 2021b). We caution that natural magmas are dynamic, evolving, open systems in which multiple generations of bubbles can nucleate during degassing, perhaps by different mechanisms. Consider a scenario in which a first wave of bubbles forms by heterogeneous nucleation, in a decompressing melt with low crystal number density, utilizing all available sites. Subsequent growth of these bubbles will degas the silicate melt, causing its liquidus temperature to increase (e.g., Hammer & Rutherford 2002), which may trigger the nucleation of new crystals, adding new nucleation sites to the system. This, in turn, may allow a second wave of heterogeneous bubble nucleation. Alternatively, if the conditions following the first nucleation wave are such that the formation of new crystals is not triggered, melt in the gaps between the sparse bubbles formed in the first wave may become sufficiently supersaturated to allow a second wave of bubble formation, this time via homogeneous nucleation. There are multiple scenarios along these lines.

Heterogeneous nucleation rates are commonly accounted for via the term α (Equation 7). We should, however, also consider the role played by the number density of crystals, or equivalently, the number density of sites for heterogeneous nucleation. For example, if the crystal number density is low, then there are only a few sites for heterogeneous nucleation, and the rest of the system is effectively a homogeneous melt. Equation 7 cannot account for this nuance; it only describes nucleation rates local to areas of abundant crystal sites only, where the number of heterogeneous nucleation sites is not limiting.

A more universally applicable approach would be to reformulate Equation 7 to accommodate the spatial control of nucleation sites. Chernov & Belof (2018) proposed an alternative heterogeneous nucleation rate law that invoked a dimensionless parameter β to account for the number density of nucleation sites. It follows that the total rate of nucleation in magma would be the sum of contributions from homogeneous nucleation rates in crystal-free regions and heterogeneous nucleation rates in the vicinity of crystals with site number density β. We therefore propose that a more general form for nucleation rate, J_T, exists, distinct from the formulation of Chernov & Belof (2018). This is the summation of rates of homogeneous and heterogeneous nucleation (potentially

over multiple crystal phases, denoted i), such that

$$J_{\mathrm{T}} = J_{\mathrm{hom}} + J_{\mathrm{het}} = J_0 \exp\left(\frac{-16\pi\sigma_\infty^3}{3k_B T(\Delta p)^2}\right) + \sum \beta_{\mathrm{i}} J_{\mathrm{i}} \exp\left(\frac{-16\pi\sigma_\infty^3}{3k_B T(\Delta p)^2}\alpha_{\mathrm{i}}\right). \quad 11.$$

The first term on the right-hand side of Equation 11 is homogeneous nucleation (Equation 4), and the second term is the sum of the contributions of each crystal phase (i) that exists in the melt. J_{i} and α_{i} are then the associated parameters for a given phase. Given that β_{i} accounts for the number density of heterogeneous nucleation sites, it is reasonable to assume that this would relate to the crystal number density and/or the crystal sizes. J_{i} could depend on these factors as well (**Figure 2**), but before now these dependencies received little attention.

3. SPONTANEOUS PHASE SEPARATION

So far, we have considered classical nucleation theory in which new gas phases (bubbles) form in response to Δp, but formation is resisted by surface tension. Recently, Allabar & Nowak (2018) found that the bubble number densities produced during decompression experiments using hydrated phonolite melts were consistently high and broadly independent of decompression rate. This is counter to classical nucleation theory, which suggests that bubble number densities should depend on decompression rate, with faster decompressions resulting in greater Δp by exceeding the rate of volatile diffusion to newly formed bubbles. Allabar & Nowak (2018) invoked spinodal decomposition—the spontaneous separation of mixtures in the absence of any energy barrier—as a tenable explanation for their observations.

Such spontaneous phase separation by uphill diffusion is driven by the mixture thermodynamics and has been investigated mainly in the case of liquid–liquid or liquid–solid separation (Cahn & Hilliard 1958, 1959; Cahn 1961, 1965; Owen & McConnell 1971; Saxena & Caneba 2002). The same process can occur for liquid–gas separation (Wedekind et al. 2009). Sahagian & Carley (2020) expanded the proposal of Allabar & Nowak (2018), exploring the possibility—and implications—of spinodal decomposition occurring in eruptible magma bodies (**Figure 3**). If supersaturated magma reaches its spinode, the work associated with bubble formation (W_{cl}) goes to zero (Debenedetti 2000), and there is no clear surface for surface tension (σ_∞) to resist phase separation (Cahn & Hilliard 1959).

As the spinode is crossed, the concept of a critical nuclear size (r_{c}) is no longer relevant, and phase separation is instead characterized by wavelength (λ). An infinite number of water concentration perturbation wavelengths are possible, but the system is unstable to any concentration fluctuations greater than a critical wavelength, λ_{c}. Instabilities with wavelength greater than λ_{c} grow at different rates; there is a sharp maximum at the fastest growing wavelength, which would lead to a relatively uniform separation distance between bubbles in magmas that undergo spinodal decomposition (**Figure 2**).

Following Hillert (1961), the differences between nucleation and spontaneous spinodal decomposition can be illustrated by examining the mechanisms in energy–amplitude–wavelength space (**Figure 4**), with wavelength being the length scale between chemical (or physical) perturbations and amplitude being the intensity of chemical perturbation. At small wavelengths homogeneous nucleation is not possible because the change in energy increases with amplitude (**Figure 4*a***). With increasing wavelength, however, the surface develops a shallow valley that deepens with wavelength and reaches zero change in energy at r_{c}. As such, homogeneous nucleation occurs only at sufficiently large size (where the characteristic wavelength is equal to or greater than r_{c}) and a sufficiently large chemical heterogeneity (indicated by amplitude). The presence of crystal surfaces can reduce the characteristic wavelength (by reducing r_{c}) and amplitude at which the

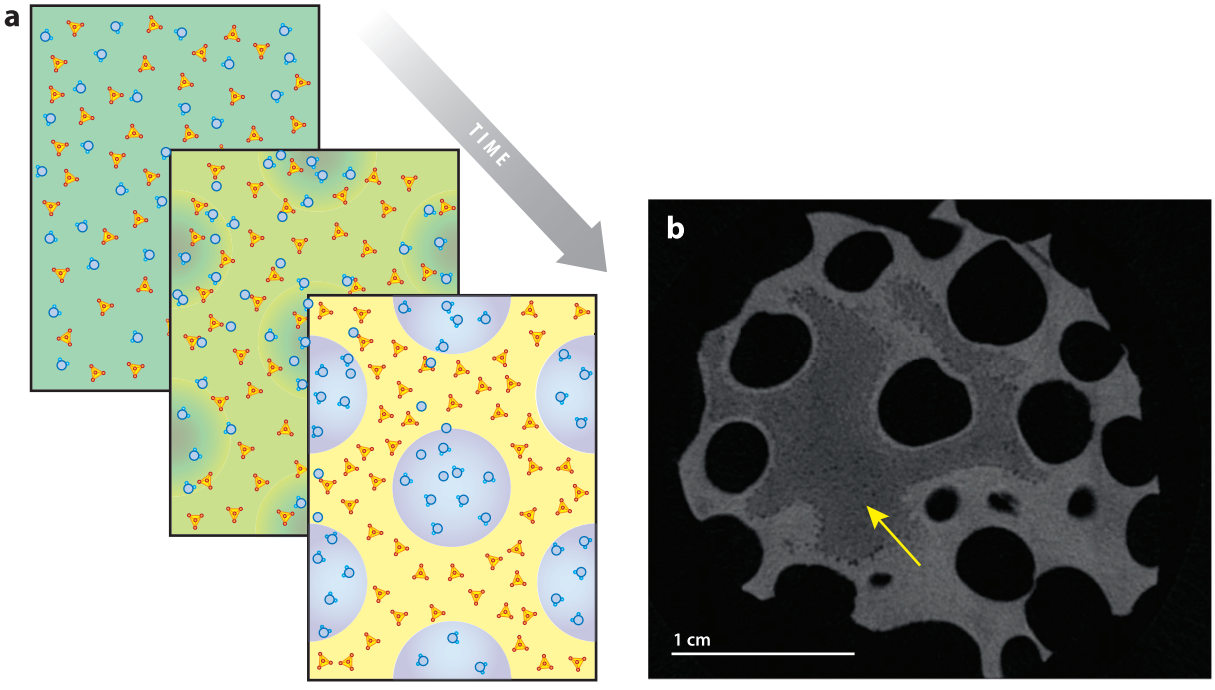

Figure 3

Spontaneous phase separation (spinodal decomposition) in hydrous silicate melts. (*a*) Following Sahagian & Carley (2020), in extreme conditions the spinode is crossed and H_2O molecules (*circles*) and silicate melt (*tetrahedrons*) unmix spontaneously into two phases. Because a given wavelength grows the fastest, a relatively uniform separation distance between bubbles will occur. (*b*) Potential spinodal decomposition of numerous small bubbles in highly H_2O-supersaturated areas in phono-tephritic silicate melt (shown by *yellow arrow*).

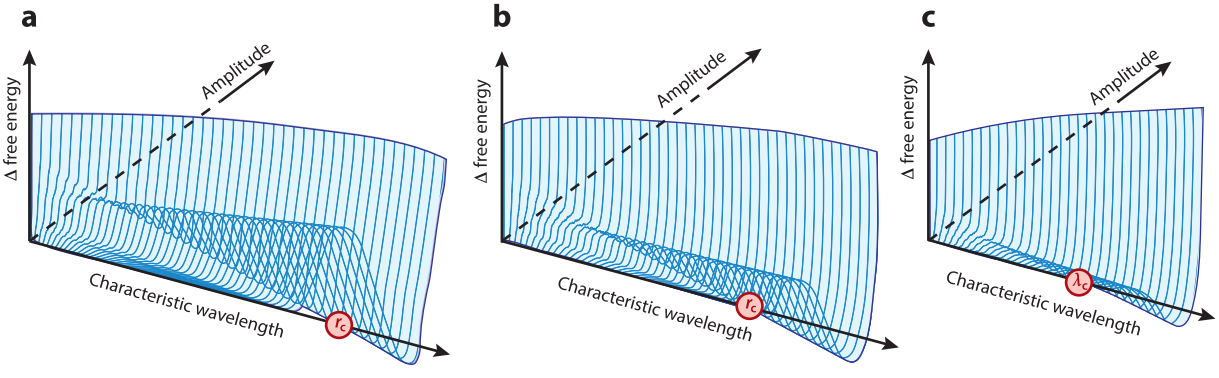

Figure 4

Energetics of bubble formation mechanisms in free energy–amplitude–wavelength space, with wavelength being the length scale between chemical perturbations and amplitude being the intensity of chemical perturbation (constructed on the concepts presented in Hillert 1961). The location of the critical nucleus size (r_c) for (*a*) homogeneous and (*b*) heterogeneous nucleation differs based on surface tension, which acts as a barrier to nucleation. Homogeneous nucleation occurs only with a sufficiently large nuclear size (characteristic wavelength) and sufficiently large chemical heterogeneity (amplitude). (*c*) Under extreme conditions the shape of the surface is altered such that no barrier exists beyond a certain wavelength (λ_c) for any chemical perturbation, and it is energetically favorable for phases to separate by spinodal decomposition.

valley reaches zero change in energy (**Figure 4*b***). Under extreme conditions, the shape of the surface is altered such that there is no potential barrier beyond a certain wavelength (**Figure 4*c***). In this case, λ_c is shorter than r_c (either homogeneous or heterogeneous), and spontaneous spinodal decomposition occurs.

Spinodal decomposition requires that a melt–volatile mixture is nonideal, such that there is strong repulsive interaction between volatile and melt species. There is evidence for this nonideality—and the existence of critical points—in rhyolites at very high pressures $p \geq 1$ GPa (Bureau & Keppler 1999). While these high pressures are not relevant for most crustal magmatic processes, there is evidence that the pressures above which H_2O–melt solutions show nonideal behavior are substantially lower for sodium-rich melts, ≥225–400 (Bureau & Keppler 1999; Sowerby & Keppler 2002; McMillan 1994). The enrichment of alkalis in phonolites relative to rhyolites opens the possibility of spinodal decomposition occurring at crustal pressures (Allabar & Nowak 2018). Preliminary experimental work with highly supersaturated phono-tephritic melt (**Figure 3*b***) supports this hypothesis. In this case, rapidly decompressed hydrous phono-tephritic melt formed two populations of bubbles. The first formed via homogeneous nucleation at ~100 MPa (large bubbles in **Figure 3*b***). A second population of highly numerous, evenly spaced, small (~1 μm) bubbles formed at ~120 MPa supersaturation. That second wave of bubbles grew within the melt that was not degassed by growth of the first bubbles. More studies of highly supersaturated peralkaline melts are needed to explore the potential of spontaneous phase separation in volcanic systems.

4. CHALLENGES TO MODELING BUBBLE NUCLEATION MECHANISMS

Many challenges remain in fully understanding the formation of gas bubbles in silicate melts, precluding the development of a general, universally applicable model. Extensive experimental work is needed to constrain the driving forces and barriers to bubble formation. Here we present three such challenges and suggest ways to close the associated knowledge gaps.

4.1. Challenge 1: Constrain Surface Tension for Silicate Melts

One of the biggest challenges to modeling bubble nucleation is defining σ_∞ appropriately for systems of interest. Discrepancies of up to many orders of magnitude occur when experimental results for J_{hom} are compared to predictions made by classical nucleation theory (Navon & Lyakhovsky 1998, Lubetkin 2003, Gonnermann & Gardner 2013, Hajimirza et al. 2019). Such discrepancies most likely result from the dependency of W_{cl} on σ_∞^3 (Equation 5); small changes in σ_∞ cause orders of magnitude change in J_{hom} (Navon & Lyakhovsky 1998). Because the kinetics of heterogeneous nucleation also depend on σ_∞ (Equation 9), having the correct value for σ_∞ is critical for modeling and quantifying the impacts of specific crystal populations.

Much of the discrepancy between experimental results and classical nucleation theory can be attributed to the capillary approximation made in classical nucleation theory that the surface of a critical nucleus is well defined and sharp (**Figure 5*a***). That approximation leads to the assumption that surface tension for the nucleus (σ_{nuc}) equals σ_∞ (Navon & Lyakhovsky 1998, Lubetkin 2003, Merikanto et al. 2007, Gonnermann & Gardner 2013). Instead, experimental results are more consistent with predictions from classical nucleation theory when the interface is assumed to be a diffuse, inhomogeneous region, such that σ_{nuc} is lower than σ_∞ (**Figure 5*b***). Gonnermann & Gardner (2013) found that homogeneous bubble nucleation in hydrous rhyolitic melt was consistent with $\sigma_{nuc} < \sigma_\infty$, with σ_{nuc} depending on Δp. This finding points to a diffuse

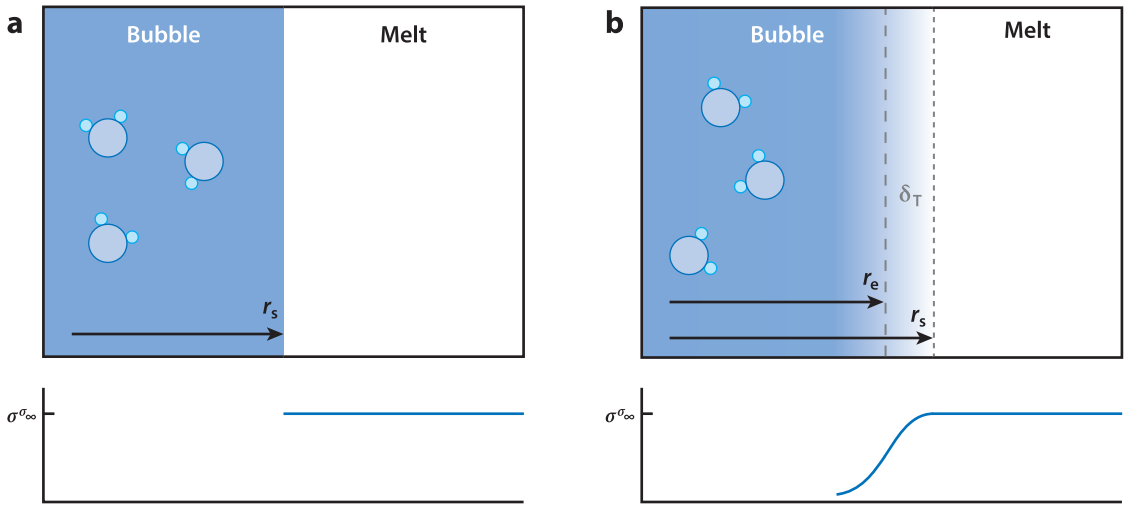

Figure 5

The characteristics of the boundary between bubble nucleus and silicate melt (see **Figure 1*a***) dictate the surface tension that is appropriate for modeling nucleation. (*a*) In classical nucleation theory, the capillary approximation leads to the assumption that the surface of the nucleus is sharp and well defined. In that case, surface tension at the interface of a nucleus with radius r_s is σ_∞ (illustrated by the *horizontal line*), the macroscopically measurable interfacial tension between the vapor phase and melt with an interface of large radius of curvature. (*b*) The interface between nucleus and melt is more likely diffuse and inhomogeneous. In this case, surface tension for the nucleus (σ_{nuc}) is lower than σ_∞ and is approximated with the Tolman distance (δ_T), which is defined by the equimolecular distance (r_e) between phases.

interface, perhaps most appropriately associated with nano-scale bubbles (Kashchiev 2003, 2004; Lubetkin 2003; Gonnermann & Gardner 2013; Hajimirza et al. 2019).

One approach to modifying surface tension for microscopic (or nano-scale) nuclei is to use the expression by Tolman (1948), which estimates the deviation of surface tension of nano-scale bubbles and droplets depending on their size. This has the form

$$\frac{\sigma_{nuc}}{\sigma_\infty} = \frac{1}{1 + 2\delta_T/r_s}, \qquad 12.$$

where r_s is the radius of a nucleus and δ_T is the Tolman length (**Figure 5*b***). In this case, σ_{nuc} is for the equimolecular surface, as defined by δ_T, which is inside the inhomogeneous region between phases (Schmelzer et al. 2019). Hajimirza et al. (2019) used experimental results for J_{hom} in rhyolitic melts to approximate δ_T and found that $\sigma_{nuc} < \sigma_\infty$ and that σ_{nuc} increased with Δp.

Despite the apparent success of modeling efforts, Hajimirza et al. (2019) were unable to obtain a functional form for σ_{nuc} as a function of Δp that matched predictions. S. Hajimirza (personal communication) speculates that this failure likely resulted from the assumption that δ_T is constant. Indeed, studies have found that the approximation proposed by Tolman (1949) is valid only for small deviations from thermodynamic equilibrium and is not sufficiently accurate to describe nucleation rates proceeding at large supersaturations (Schmelzer et al. 1996, 2019; Baidakov & Boltachev 1999; Baidakov et al. 2000; Lei et al. 2005; Joswiak et al. 2013). Others (Schmelzer 1986, Schmelzer & Mahnke 1986) have proposed a more general formula to describe the effect of cluster size on σ_{nuc}, showing that the results of Tolman (1948) and others can be obtained as special cases. Experimental data for nucleation rates of bubbles in silicate melts have not been used to test the validity for this general formula, so presently no functional form for $\sigma_{nuc}(\Delta p)$ exists that is consistent with the physics for interfaces in silicate melts.

Although having a functional form for $\sigma_{nuc}(\Delta p)$ is required to model bubble nucleation, it cannot be fully determined without knowing the macroscopic value σ_∞ (Equation 12). It is known that σ_∞ varies as a function of melt composition, temperature, and importantly H_2O content (Bagdassarov et al. 2000). Limited data exist, however, for hydrous silicate melts across the full compositional spectrum of erupted magmas. For anhydrous silicate melts, σ_∞ has been derived mainly from deformation of hot melt drops (Walker & Mullins 1981, Bagdassarov et al. 2000). When results are corrected for temperature differences, Walker & Mullins (1981) and Bagdassarov et al. (2000) found that σ_∞ for anhydrous melts ranging from limburgite (SiO_2 contents of 43.3 wt%) to rhyolite (SiO_2 = 75.6 wt%) vary little and fall within a range from 0.344 to 0.359 N m^{-1}. Temperature impacts σ_∞, with results for a range of melt compositions indicating that σ_∞ increases with temperature, with a dependence of ~2–7 × 10^{-5} N m^{-1} K^{-1} (Walker & Mullins 1981, Bagdassarov et al. 2000).

Very few data exist for σ_∞ for hydrous silicate melts. Gardner et al. (2013) nucleated bubbles in hydrous silicate melts that had ~4 wt% dissolved H_2O but differed in SiO_2 content by up to 25 wt%. They found that the relative difference in surface tension must have been small, similar to that of anhydrous melts. To date, however, σ_∞ has only been measured directly for hydrous haplogranite melt at 1,000°C (Bagdassarov et al. 2000). In this case, σ_∞ was found to decrease significantly from 0.270 N m^{-1} at 0.1 MPa to 0.065 N m^{-1} at 400 MPa, spanning H_2O contents from ~0 wt% to 10.4 wt%. This variation is used in many models of bubble nucleation (e.g., Massol & Koyaguchi 2005; Toramaru 2006, 2014; Hajimirza et al. 2019, 2021a,b). The results need to be tested and confirmed, however, because Bagdassarov et al. (2000) found substantially lower values of σ_∞ (0.281–0.284 N m^{-1}) for anhydrous haplogranitic melt compared to all natural melt compositions measured (Walker & Mullins 1981, Bagdassarov et al. 2000).

We propose that future work in this area should do the following:

1. Measure σ_∞ as a function of composition, pressure, and temperature, over the ranges relevant to natural magmatic systems, and develop a quantitative and general model for σ_∞.
2. Develop a general expression for the effective surface tension for small bubble nuclei σ_{nuc} as a function of macroscopic surface tension σ_∞ and the conditions of bubble formation.

4.2. Challenge 2: Constrain Microphysics of Nucleation on Heterogeneities

Studies of heterogeneous nucleation have found that different crystal phases are variably effective at enhancing bubble nucleation in different compositions of melt (see Section 2.2) and under different nucleation conditions. In the case of rhyolitic melts, magnetite is the only phase that is highly effective at enhancing nucleation (Hajimirza et al. 2021b). Hurwitz & Navon (1994) showed that the efficiency of nucleation on magnetite increased with increased Δp, with bubbles nucleating at $\Delta p < 5$ MPa on 50–60% of the magnetite crystals present, but on >90% of them when $\Delta p > 30$ MPa. Gardner & Denis (2004) showed that one to a few bubbles nucleated on faces of magnetite at low Δp, but multiple bubbles nucleated on single magnetite grains at high Δp. The number and location of bubble nucleation on individual hematite grains also increased as Δp increased.

Such observations demonstrate that different sites and different numbers of sites on crystals activate under different conditions, and thus the number density of bubbles generated through heterogeneous nucleation can differ profoundly depending on the dynamics of magma decompression. To advance our quantitative modeling of heterogeneous nucleation, we need to develop

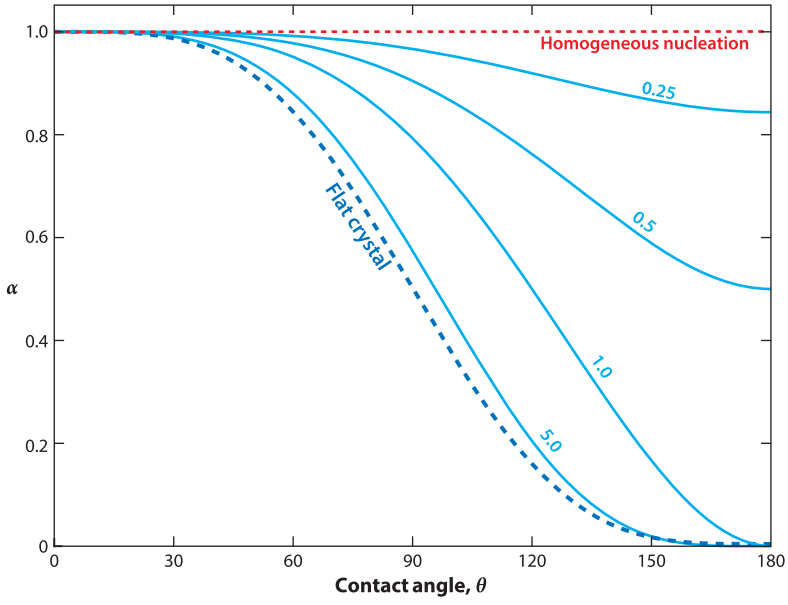

Figure 6

Effect of crystal curvature on efficiency as a nucleation site. The dashed dark blue curve shows the $\alpha(\theta)$ relationship for flat surfaces (Equation 8). Solid light blue curves show the same relationship for crystals with different radii of curvature, expressed as values of R/r_c, which is the ratio between the crystal radius of curvature R and the critical nucleus size. As R/r_c decreases, crystals become less effective nucleation sites. Homogeneous nucleation is shown as the dashed red curve.

a more complete quantitative understanding of how the effectiveness of different crystal phases as nucleation sites is influenced by the sizes, shapes, and abundance of crystals, under different conditions of bubble formation.

The simple model for heterogeneous nucleation discussed so far assumes that the surface is flat. Bubble nucleation, however, often takes place on micron- and nano-scale crystals, where the surface curvature can become comparable to the critical nucleus size, and on complex crystals, where the critical nucleus is comparable to the size of the steps and corners on the crystals. Indeed, several authors (e.g., Fletcher 1958, Qian & Ma 2009) have studied nucleation on convex spherical surfaces and found that the α term has a complex dependence on both the contact angle and the surface radius of curvature (**Figure 6**). In particular, the nucleation energy barrier increases as the crystal size becomes smaller, hence $\alpha \rightarrow 1$ as crystals get smaller. These results contrast with recent studies of natural volcanic products that suggest nanolites (crystals ≤ 1 μm in size) may serve as sites for bubble nucleation (e.g., Mujin & Nakamura 2014; Di Genova et al. 2018, 2020; Cáceres et al. 2020; Colombier et al. 2020; Knafelc et al. 2022).

The formulation for heterogeneous nucleation proposed in this review (Equation 11) includes β_i, J_i, and α_i for each phase. By design, β_i is a scaling factor that allows the number density of crystals to be incorporated into the J_{het} rate. Both β_i and J_i could reasonably depend on the size of crystals because more than one bubble can nucleate on a given crystal (Gardner & Denis 2004), and crystal size may influence the number of nucleation sites available. As per Equation 8, α_i is geometric and depends on θ, but is for a bubble on a flat crystal surface. In the case of magnetite—often formed as nano-scale crystals—the flat interfaces of the crystal are unlikely to host a single

bubble without the bubble–crystal contact involving the corners or nonflat portions of the crystal. For example, nucleation has been found to be favored at concave corners because of the presence of additional crystal–bubble interfaces (Hurwitz & Navon 1994, Page & Sear 2006, Hedges & Whitelam 2012, Yang et al. 2022). As such, future research should acknowledge that α_i as given by Equation 8 is insufficient as bubble sizes approach crystal nucleation site sizes, and a modified α_i for corner or curved sites would be needed (Fletcher 1958, Page & Sear 2006, Qian & Ma 2009, Hedges & Whitelam 2012, Yang et al. 2022). For example, on a curved site, α_i becomes (Fletcher 1958, Qian & Ma 2009)

$$\alpha_i = \frac{1}{2}\left(1 - \left(\frac{\chi\cos\theta - 1}{g}\right)^3 + \chi^3\left(2 - 3\left(\frac{\chi - \cos\theta}{g}\right) + \left(\frac{\chi - \cos\theta}{g}\right)^3\right)\right) + 3\cos\theta\chi^2\left(1 - \frac{\chi - \cos\theta}{g}\right), \quad 13.$$

where $\chi = R/r_c$ is the ratio between the crystal radius of curvature R and the critical nucleus size and $g = \sqrt{1 + \chi^2 + 2\cos\theta\chi}$. For a given crystal shape, therefore, a bulk effective α_i would change as a function of the ratio of crystal size to bubble nucleus size.

We propose that future work in this area should do the following:

1. Constrain the number of nucleation sites on crystals of different phases, shapes, and sizes, under different conditions of bubble formation, and use these data to develop a model for the microphysics of bubble nucleus formation on crystals with typical natural habits.
2. Determine for different crystal phases the dependence of the factors J_i, β_i, and α_i (Equation 11) on crystal size and shape, including the presence of steps and corners.

4.3. Challenge 3: Interpret Bubble Formation Histories from Natural Eruptive Products

The record of degassing preserved as vesicles in volcanic products challenges the experimental and modeling communities to better constrain the mechanisms of nucleation. Consider that both rhyolitic (high silica content and high viscosity) and phonolitic (low silica content and generally low viscosity) magmas can produce highly explosive Plinian eruptions. Products of phonolitic eruptions often have significantly higher bubble number densities than their rhyolitic counterparts (**Figure 7**). These differences span wide ranges in eruption mass flux, crystal content, and melt volatile content, and they cannot be explained by variable pre-eruptive conditions alone. Instead, they may reflect contrasting bubble nucleation mechanisms.

Consider very fine ash, which constitutes the majority of particles generated by explosive eruptions. Ash often preserves bimodal bubble size populations, with the smaller bubbles thought to reflect a second nucleation event (e.g., Toramaru 2014) that occurred just prior to fragmentation (Proussevitch et al. 2011; Genareau et al. 2012, 2013). Experimental and modeling studies that attempt to replicate such textures typically restrict nucleation to one mechanism (e.g., Toramaru 1989, 2006, 2014; Massol & Koyaguchi 2005; Cluzel et al. 2008; Hamada et al. 2010; Le Gall & Pichavant 2016a). That assumption leads to the need for dramatic changes in other parameters (decompression rate, etc.) in order to allow conditions to be reestablished to trigger subsequent nucleation events.

We should consider the possibility that multiple nucleation mechanisms may occur simultaneously and sequentially before, and during, explosive eruptions (Equation 11). Using this more nuanced approach, the number density and resulting size distribution of vesicles in natural volcanic

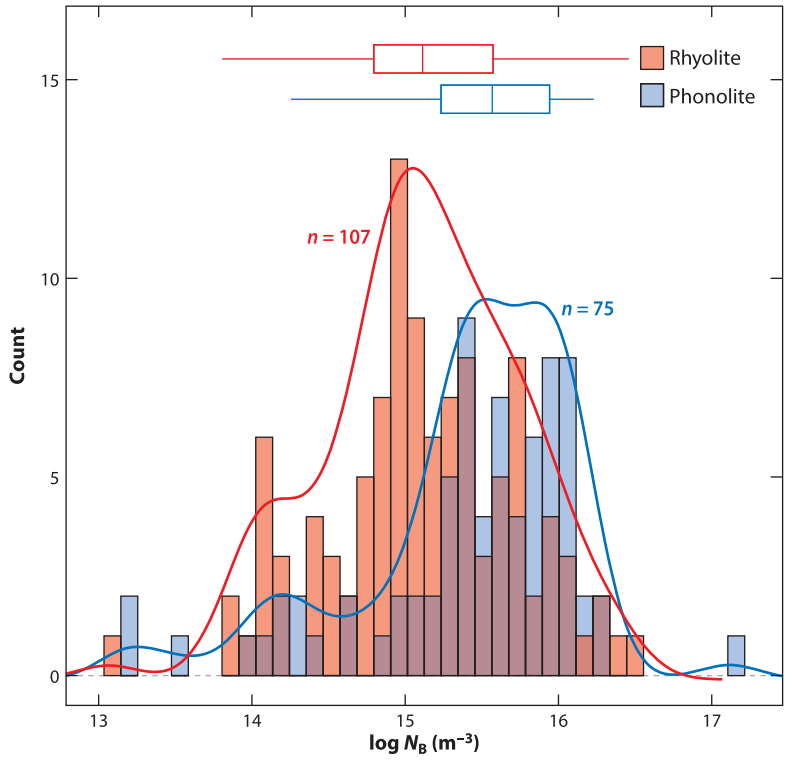

Figure 7

Histogram of measured vesicle (bubble) number densities (N_B) for pumice samples from rhyolitic and phonolitic explosive eruptions (composition on a whole-rock basis) (data compiled in Cáceres et al. 2020; see references within). Also shown are the kernel density estimates (*curves*) and the box-and-whisker plots displaying the mean and the upper and lower quartiles.

products can be interpreted as the summation of bubbles formed via all available mechanisms (homogeneous, heterogeneous, and/or spinodal decomposition). The rate of bubble nucleation (J) is described in terms of numbers per volume of melt per unit time (Equations 7 and 11) because new nucleation sites appear stochastically within a volume of melt. The cumulative number density of bubbles (N_B) formed by homogeneous and heterogeneous bubble nucleation will thus be given by

$$N_B = \int_{t_1}^{t_2} J_T \, dt, \qquad 14.$$

where $t_2 - t_1$ is the time allowed for nucleation, which would be that over which decompression and magma ascent occur. At the same time, bubbles could form through spinodal decomposition, with a spatial distribution determined by the wavelength of the fastest growing instability, anywhere in the melt where the appropriate conditions were met. During ascent, a complex history of bubble formation is possible, and entertaining multiple mechanisms for nucleation events is critical to fully evaluating the degassing pathway followed by magma.

It must be stressed, however, that the numbers and sizes of bubbles preserved as vesicles in volcanic products do not reflect solely nucleation events. Nucleation instead is just the first step in a chain of events that includes bubble growth, coalescence, resorption, percolation via the onset of permeability, and outgassing-driven collapse, all of which result in the final vesicle textures seen.

Bubbles grow by volatile diffusion and decompression, which can locally deplete volatiles from the melt surrounding the bubbles and effectively halt nucleation. The post-nucleation growth of individual bubbles in silicate melts is relatively well understood (Proussevitch et al. 1993; Proussevitch & Sahagian 1996, 1998; Blower et al. 2001; Lensky et al. 2004; Chernov et al. 2018; Coumans et al. 2020), but most growth models do not explicitly include the nucleation step. Therefore, most existing models do not account for the complex evolution of N_B and bubble size distribution that can result from multiple nucleation events, or even a single nucleation event with spatially irregular nucleation sites. In fact, the nucleation mechanism controls not only the initial distribution of bubbles but also the conditions under which bubbles will grow and interact to create a final N_B and bubble size distribution that can be observed in eruption products (e.g., Castro et al. 2012, McIntosh et al. 2014). It is thus clear that advancements are also needed to model the full evolution of gas bubbles in magmas in order to utilize measured vesicle populations to infer volcanic processes.

We propose that future work in this area should do the following:

1. Create a general model for bubble nucleation and bubble growth that allows for the style of bubble formation mechanism to change over time in response to evolving local conditions, including local variations in pressure–temperature–composition within the magma.
2. Use such a model to explore bubble formation and growth under realistic pressure–temperature–time pathways in order to link bubble textures observed in natural pyroclasts to conditions experienced during transport and eruption.
3. Ultimately, integrate a general, validated model for bubble formation and growth with numerical conduit and eruption models. This will enable more accurate modeling of the two-way coupling between magma transport and bubble growth.

5. CAUTIONARY WORDS FOR FUTURE EXPERIMENTAL STUDIES

Significant experimental work is needed to understand bubble formation in silicate melts over the full spectra of melt and volatile compositions, under various Δp conditions. These experiments should include decompressions of both superliquidus (melt–fluid only) and subliquidus (crystal-bearing) silicate melts. Attention should be paid to the style of decompression because that impacts the outcome, with sudden step-wise decompression producing different N_B and bubble size distributions compared to continuous decompression (e.g., Nowak et al. 2011, Fiege & Cichy 2015). Rapid, single-step decompression experiments offer relatively straightforward measurements of nucleation rates (Hajimirza et al. 2019, 2021a,b). In contrast, interpretation of the N_B and bubble size distributions for continuous decompression experiments must account for the complexity of the degassing pathway, encapsulated in Equation 14, in order for useful information concerning nucleation rates to be extracted. All decompression experiments, regardless of decompression path, can suffer from bubble resorption and rehydration during cooling of the experimental silicate melt (McIntosh et al. 2014). To fully understand nucleation processes, the experimental community should seek methods that avoid post-nucleation complications as much as possible.

6. SUMMARY

Volcanic eruptions are driven by volatiles coming out of solution and forming bubbles in ascending magmas. Extensive experimental and numerical work over the past 30 years has been carried out to understand the mechanisms of bubble formation. It is known that bubbles can form in magmas via homogeneous nucleation and heterogeneous nucleation on crystal surfaces, and possibly also spontaneous phase separation via spinodal decomposition. We propose a general approach

for calculating bubble nucleation rates as the sum of the contributions from homogeneous nucleation and heterogeneous nucleation, suggesting that nucleation may not be limited to a single mechanism prior to eruption. Despite the numerous studies on bubble formation, there remain significant gaps in our knowledge before the development of a general model for bubble formation under natural eruption conditions can be implemented. We propose that three major challenges are constraining surface tension for silicate melts, analyzing the microphysics of nucleation on heterogeneities, and interpreting bubble formation histories from natural eruptive products. By overcoming these challenges, we hope that the volcanological community will be better able to infer eruptive mechanisms and magma degassing at depth.

DISCLOSURE STATEMENT

The authors are not aware of any affiliations, memberships, funding, or financial holdings that might be perceived as affecting the objectivity of this review.

ACKNOWLEDGMENTS

We are grateful to the many who have discussed bubble dynamics and magma degassing with us. J.E.G. received funding from US National Science Foundation grant (EAR) 1725186. F.B.W. received funding from UK Natural Environment Research Council grant NE/T007796/1. E.W.L. and D.S. received funding from Royal Society International Exchanges grant IES\R1\191001. E.W.L. received funding from UK Natural Environment Research Council grant NE/N002954/1.

LITERATURE CITED

Allabar A, Nowak M. 2018. Message in a bottle: spontaneous phase separation of hydrous Vesuvius melt even at low decompression rates. *Earth Planet. Sci. Lett.* 501:192–201

Alletti M, Baker DR, Freda C. 2007. Halogen diffusion in a basaltic melt. *Geochim. Cosmochim. Acta* 71:3570–80

Allison CM, Roggensack K, Clarke AB. 2022. MafiCH: a general model for H_2O-CO_2 solubility in mafic melts. *Contrib. Mineral. Petrol.* 177:40

Applegarth LJ, Tuffen H, James MR, Pinkerton H, Cashman KV. 2013. Direct observations of degassing-induced crystallization in basalts. *Geology* 41:243–46

Bagdassarov N, Dorfman A, Dingwell D. 2000. Effect of alkalis, phosphorus, and water on the surface tension of haplogranite melt. *Am. Mineral.* 85:33–40

Baidakov VG, Boltachev GS. 1999. Curvature dependence of the surface tension of liquid and vapor nuclei. *Phys. Rev. E* 59:469–75

Baidakov VG, Boltashev GS, Schmelzer JWP. 2000. Comparison of different approaches to the determination of the work of critical cluster formation. *J. Colloid Interface Sci.* 231:312–21

Blake S. 1984. Volatile oversaturation during the evolution of silicic magma chambers as an eruption trigger. *J. Geophys. Res.* 89(B10):8237–44

Blank JG, Stolper EM, Carroll MR. 1993. Solubility of carbon dioxide and water in rhyolitic melt at 850°C and 750 bars. *Earth Planet. Sci. Lett.* 119:27–36

Blower JD, Mader HM, Wilson SDR. 2001. Coupling of viscous and diffusive controls on bubble growth during explosive volcanic eruptions. *Earth Planet. Sci. Lett.* 193:47–56

Bureau H, Keppler H. 1999. Complete miscibility between silicate melts and hydrous fluids in the upper mantle: experimental evidence and geochemical implications. *Earth Planet. Sci. Lett.* 165:187–96

Cáceres F, Wadsworth FB, Scheu B, Colombier M, Madonna C, et al. 2020. Can nanolites enhance eruption explosivity? *Geology* 48:997–1001

Cahn JW. 1961. On spinodal decomposition. *Acta Metall.* 9:795–801

Cahn JW. 1965. Phase separation by spinodal decomposition in isotropic systems. *J. Chem. Phys.* 42:93–99

Cahn JW, Hilliard JE. 1958. Free energy of a nonuniform system. I. Interfacial free energy. *J. Chem. Phys.* 28:258–67

Cahn JW, Hilliard JE. 1959. Free energy of a nonuniform system. III. Nucleation in a two-component incompressible fluid. *J. Chem. Phys.* 31:688–99

Carroll MR, Webster JD. 1994. Solubilities of sulfur, noble gases, nitrogen, chlorine and fluorine in magmas. *Rev. Mineral. Geochem.* 30:231–79

Castro JM, Burgisser A, Shipper I, Mancini S. 2012. Mechanisms and dynamics of bubble coalescence in silicic magmas. *Bull. Volcanol.* 74:2339–52

Chernov AA, Belof JL. 2018. *Homogeneous versus heterogeneous nucleation modes of solidification at strong driving force conditions*. Rep. LLNL-TR-751938, Lawrence Livermore Natl. Lab., Livermore, CA

Chernov AA, Pil'nik AA, Davydov MN, Ermanyuk EV, Pakhomov MA. 2018. Gas nucleus growth in high-viscosity liquid under strongly non-equilibrium conditions. *Int. J. Heat Mass Transf.* 123:1101–8

Cichy SB, Botcharnikov RE, Holtz F, Behrens H. 2011. Vesiculation and microlite crystallization induced by decompression: a case study of the 1991–1995 Mt Unzen eruption (Japan). *J. Petrol.* 52:1469–92

Cluzel N, Laporte D, Provost A, Kannewischer I. 2008. Kinetics of heterogeneous bubble nucleation in rhyolitic melts: implications for the number density of bubbles in volcanic conduits and for pumice textures. *Contrib. Mineral. Petrol.* 156:745–63

Colombier M, Shea T, Burgisser A, Druitt TH, Gurioli L, et al. 2020. Rheological change and degassing during a trachytic Vulcanian eruption at Kilian Volcano, Chaîne des Puys, France. *Bull. Volcanol.* 82:78

Couch S, Sparks RSJ, Carroll MR. 2003. The kinetics of degassing-induced crystallization at Soufrière Hills volcano, Montserrat. *J. Petrol.* 44:1477–502

Coumans J, Llewellin E, Wadsworth F, Humphreys M, Mathias SA, et al. 2020. An experimentally validated numerical model for bubble growth in magma. *J. Volcanol. Geotherm. Res.* 402:107002

Debenedetti PG. 1996. *Metastable Liquids: Concepts and Principles*. Princeton, NJ: Princeton Univ. Press

Debenedetti PG. 2000. Phase separation by nucleation and by spinodal decomposition: fundamentals. *Supercrit. Fluids* 366:123–66

Di Genova D, Brooker RA, Mader HM, Drewitt JWE, Longo A, et al. 2020. In situ observation of nanolite growth in volcanic melt: a driving force for explosive eruptions. *Sci. Adv.* 6:eabb0413

Di Genova D, Caracciolo A, Kolzenburg S. 2018. Measuring the degree of "nanotilization" of volcanic glasses: understanding syn-eruptive processes recorded in melt inclusions. *Lithos* 318:209–18

Di Matteo V, Carroll MR, Behrens H, Vetere F, Brooker RA. 2004. Water solubility in trachytic melts. *Chem. Geol.* 213:187–96

Dixon JE. 1997. Degassing of alkalic basalts. *Am. Mineral.* 82:368–78

Dixon JE, Stolper EM, Holloway JR. 1995. An experimental study of water and carbon dioxide solubilities in mid-ocean ridge basaltic liquids. Part I: calibration and solubility models. *J. Petrol.* 36:1607–31

Epel'baum MB. 1973. Surface tension of felsic magmatic melts at high temperatures and pressure. *Geochem. Int.* 10:343–45

Fiege A, Cichy SB. 2015. Experimental constraints on bubble formation and growth during magma ascent. *Am. Mineral.* 100:2426–42

Fiege A, Holtz F, Cichy SB. 2014. Bubble formation during decompression of andesitic melts. *Am. Mineral.* 99:1052–62

Fletcher NH. 1958. Size effect in heterogeneous nucleation. *J. Chem. Phys.* 29:572–76

Fogel RA, Rutherford MJ. 1990. The solubility of carbon dioxide in rhyolitic melts; a quantitative FTIR study. *Am. Mineral.* 75:1311–26

Freda C, Baker DR, Scarlato P. 2005. Sulfur diffusion in basaltic melts. *Geochim. Cosmochim. Acta* 69:5061–69

Gardner JE. 2007. Heterogeneous bubble nucleation in highly viscous silicate melts during instantaneous decompression from high pressure. *Chem. Geol.* 236:1–12

Gardner JE. 2012. Surface tension and bubble nucleation in phonolite magmas. *Geochim. Cosmochim. Acta* 76:93–102

Gardner JE, Denis M-H. 2004. Heterogeneous bubble nucleation on Fe-Ti oxide crystals in high-silica rhyolitic melts. *Geochim. Cosmochim. Acta* 68:3587–97

Gardner JE, Hajimirza S, Webster JD, Gonnermann HM. 2018. The impact of dissolved fluorine on bubble nucleation in hydrous rhyolite melts. *Geochim. Cosmochim. Acta* 226:174–81

Gardner JE, Ketcham RA. 2011. Bubble nucleation in rhyolite and dacite melts: temperature dependence of surface tension. *Contrib. Mineral. Petrol.* 162:929–43

Gardner JE, Ketcham RA, Moore G. 2013. Surface tension of hydrous silicate melts: constraints on the impact of melt composition. *J. Volcanol. Geotherm. Res.* 267:68–74

Gardner JE, Webster JD. 2016. The impact of dissolved CO_2 on bubble nucleation in water-poor rhyolite melts. *Chem. Geol.* 420:180–85

Genareau K, Mulukutla GK, Proussevitch AA, Durant AJ, Rose WI, Sahagian DL. 2013. The size range of bubbles that produce ash during explosive volcanic eruptions. *J. Appl. Volcanol.* 2:4

Genareau K, Proussevitch AA, Durant AJ, Mulukutla G, Sahagian DL. 2012. Sizing up the bubbles that produce very fine ash during explosive volcanic eruptions. *Geophys. Res. Lett.* 39:L15306

Ghiorso MS, Gualda GAR. 2015. An H_2O–CO_2 mixed fluid saturation model compatible with rhyolite-MELTS. *Contrib. Mineral. Petrol.* 169:53

Gibbs JW. 1961. Influence of Surfaces of Discontinuity upon the Equilibrium of Heterogeneous Masses—Theory of Capillarity. In *The Scientific Papers of J. Willard Gibbs*, Vol. 1: *Thermodynamics*, pp. 219–331. New York: Dover

Girona T, Costa F, Schubert G. 2016. Degassing during quiescence as a trigger of magma ascent and volcanic eruptions. *Sci. Rep.* 5:18212

Gondé C, Martel C, Pichavant M, Bureau H. 2011. In situ bubble vesiculation in silicic magmas. *Am. Mineral.* 96:111–24

Gonnermann HM, Gardner JE. 2013. Homogeneous bubble nucleation in rhyolitic melt: experiments and non-classical theory. *Geochem. Geophys. Geosyst.* 14:4758–73

Hajimirza S, Gardner JE, Gonnermann HM. 2021a. Experimental demonstration of continuous bubble nucleation in rhyolite. *J. Volcanol. Geotherm. Res.* 421:107417

Hajimirza S, Gonnermann HM, Gardner JE. 2021b. Reconciling bubble nucleation in explosive eruptions with geospeedometers. *Nat. Comm.* 12:283

Hajimirza S, Gonnermann HM, Gardner JE, Giachetti T. 2019. Predicting homogeneous bubble nucleation in rhyolite. *J. Geophys. Res. Solid Earth* 124:2395–416

Hamada M, Laporte D, Cluzel N, Koga KT, Kawamoto T. 2010. Simulating bubble number density of rhyolitic pumices from Plinian eruptions: constraints from fast decompression experiments. *Bull. Volcanol.* 72:735–46

Hammer JE, Rutherford MJ. 2002. An experimental study of the kinetics of decompression-induced crystallization in silicic melt. *J. Geophys. Res.* 107(B1):ECV-8-1–8-24

Hardiagon M, Laporte D, Marizet Y, Provost A. 2013. CO_2 degassing in a haplo-basaltic magma: an experimental approach. *Mineral. Mag.* 77:1258

Hedges LO, Whitelam S. 2012. Patterning a surface so as to speed nucleation from solution. *Soft Matter* 8:8624–35

Hess K-U, Dingwell DB. 1996. Viscosities of hydrous leucogranitic melts: a non-Arrhenian model. *Am. Mineral.* 81:1297–300

Hillert M. 1961. A solid-solution model for inhomogeneous systems. *Acta Metal.* 9:525–35

Hirth JP, Pound GM, Pierre GRS. 1970. Bubble nucleation. *Metal. Trans.* 1:939–45

Holtz F, Behrens H, Dingwell DB, Johannes W. 1995. H_2O solubility in haplogranitic melts: compositional, pressure, and temperature dependence. *Am. Mineral.* 80:94–108

Hurwitz S, Navon O. 1994. Bubble nucleation in rhyolitic melts: experiments at high pressure, temperature, and water content. *Earth Planet. Sci. Lett.* 122:267–80

Iacono-Marziano G, Morizet Y, Le Trong E, Gaillard F. 2012. New experimental data and semi-empirical parameterization of H_2O–CO_2 solubility in mafic melts. *Geochim. Cosmochim. Acta* 97:1–23

Iacono-Marziano G, Schmidt BC, Dolfi D. 2007. Equilibrium and disequilibrium degassing of a phonolitic melt (Vesuvius AD 79 "white pumice") simulated by decompression experiments. *J. Volcanol. Geotherm. Res.* 161:151–64

Johnson MC, Anderson AT, Rutherford MJ. 1994. Pre-eruptive volatile contents of magmas. *Rev. Mineral. Geochem.* 30:281–330

Joswiak MN, Duff N, Doherty MF, Peters P. 2013. Size-dependent surface free energy and Tolman-corrected droplet nucleation of TIP4P/2005 water. *J. Phys. Chem. Lett.* 4:4267–72

Jugo PJ, Luth RW, Richards JP. 2005. An experimental study of the sulfur content in basaltic melts saturated with immiscible sulphide or sulfate liquids at 1300°C and 1.0 GPa. *J. Petrol.* 46:783–98

Kashchiev D. 2000. *Nucleation: Basic Theory with Applications*. Oxford, UK: Elsevier

Kashchiev D. 2003. Thermodynamically consistent description of the work to form a nucleus of any size. *J. Chem. Phys.* 118:1837–51

Kashchiev D. 2004. Multicomponent nucleation: thermodynamically consistent description of the nucleation work. *J. Chem. Phys.* 120:3749–58

Knafelc J, Bryan SE, Jones MWM, Gust D, Mallmann G, et al. 2022. Havre 2012 pink pumice is evidence of a short-lived, deep-sea, magnetite nanolite-driven explosive eruption. *Commun. Earth Environ.* 3:19

Landau LD, Lifshitz EM. 1980. *Statistical Physics*, Vol. 1. New York: Pergamon

Larsen JF. 2008. Heterogeneous bubble nucleation and disequilibrium H_2O exsolution in Vesuvius K-phonolite melts. *J. Volcanol. Geotherm. Res.* 175:278–88

Le Gall N, Pichavant M. 2016a. Experimental simulation of bubble nucleation and magma ascent in basaltic systems: implications for Stromboli volcano. *Am. Mineral.* 101:1967–85

Le Gall N, Pichavant M. 2016b. Homogeneous bubble nucleation in H_2O- and H_2O-CO_2-bearing basaltic melts: results of high temperature decompression experiments. *J. Volcanol. Geotherm. Res.* 327:604–21

Lei YA, Bykov T, Yoo S, Zeng XC. 2005. The Tolman length: Is it positive or negative? *J. Am. Chem. Soc.* 127:15346–47

Lensky NG, Navon O, Lyakhovsky V. 2004. Bubble growth during decompression of magma: experimental and theoretical investigation. *J. Volcanol. Geotherm. Res.* 129:7–22

Lesne P, Scaillet B, Pichavant M, Beny J-M. 2011. The carbon dioxide solubility in alkali basalts: an experimental study. *Contrib. Mineral. Petrol.* 162:153–68

Liu Y, Zhang Y, Behrens H. 2005. Solubility of H_2O in rhyolitic melts at low pressures and a new empirical model for mixed H_2O–CO_2 solubility in rhyolitic melts. *J. Volcanol. Geotherm. Res.* 143:219–35

Lubetkin SD. 2003. Why is it much easier to nucleate gas bubbles than theory predicts? *Langmuir* 19:2575–87

Luhr JF. 1990. Experimental phase relations of water- and sulfur-saturated arc magmas and the 1982 eruptions of El Chichon volcano. *J. Petrol.* 31:1071–114

Mangan M, Sisson T. 2000. Delayed, disequilibrium degassing in rhyolite magma: decompression experiments and implications for explosive volcanism. *Earth Planet. Sci. Lett.* 183:441–55

Mangan M, Sisson T. 2005. Evolution of melt-vapor surface tension in silicic volcanic systems: experiments with hydrous melts. *J. Geophys. Res.* 110(B1):B01202

Mangan MT, Sisson TW, Hankins WB. 2004. Decompression experiments identify kinetic controls on explosive silicic eruptions. *Geophys. Res. Lett.* 31:L08605

Massol H, Koyaguchi T. 2005. The effect of magma flow on nucleation of gas bubbles in a volcanic conduit. *J. Volcanol. Geotherm. Res.* 143:69–88

McIntosh IM, Llewellin EW, Humphreys MCS, Nichols ARL, Burgisser A, et al. 2014. Distribution of dissolved water in magmatic glass records growth and resorption of bubbles. *Earth Planet. Sci. Lett.* 401:1–11

McMillan P. 1994. Water solubility and speciation models. *Rev. Mineral. Geochem.* 30:131–56

Merikanto J, Zapadinsky E, Lauri A, Vehkamaki H. 2007. Origin of the failure of classical nucleation theory: incorrect description of the smallest clusters. *Phys. Rev. Lett.* 98:145702

Moore G, Vennemann T, Carmichael ISE. 1998. An empirical model for the solubility of H_2O in magmas to 3 kilobars. *Am. Mineral.* 83:36–42

Moune S, Holtz F, Botcharnikov RE. 2009. Sulphur solubility in andesitic to basaltic melts: implications for Hekla volcano. *Contrib. Mineral. Petrol.* 157:691–707

Mourtada-Bonnefoi CC, Laporte D. 1999. Experimental study of homogeneous bubble nucleation in rhyolitic magmas. *Geophys. Res. Lett.* 26:3505–8

Mourtada-Bonnefoi CC, Laporte D. 2002. Homogeneous bubble nucleation in rhyolitic magmas: an experimental study of the effect of H_2O and CO_2. *J. Geophys. Res.* 107(B4):ECV 2-1–2-19

Mourtada-Bonnefoi CC, Laporte D. 2004. Kinetics of bubble nucleation in a rhyolitic melt: an experimental study of the effect of ascent rate. *Earth Planet. Sci. Lett.* 218:521–37

Mujin M, Nakamura M. 2014. A nanolite record of eruption style transition. *Geology* 42:611–14

Navon O, Lyakhovsky V. 1998. Vesiculation processes in silicic magmas. *Geol. Soc. Lond. Spec. Publ.* 145:27–50
Newman S, Lowenstern JB. 2002. VolatileCalc: a silicate-melt–H_2O–CO_2 solution model written in Visual Basic for Excel. *Comp. Geosci.* 28:597–604
Nowak M, Cichy SB, Botcharnikov RE, Walker N, Hurkuck W. 2011. A new type of high-pressure low-flow metering valve for continuous decompression: first experimental results on degassing of rhyodacitic melts. *Am. Mineral.* 96:1373–80
Owen DC, McConnell JDC. 1971. Spinodal behaviour in an alkali feldspar. *Nat. Phys. Sci.* 230:118–19
Page AJ, Sear RP. 2006. Heterogeneous nucleation in and out of pores. *Phys. Rev. Lett.* 97:065701
Papale P, Moretti R, Barbato D. 2006. The compositional dependence of the saturation surface of H_2O + CO_2 fluids in silicate melts. *Chem. Geol.* 229:78–95
Pichavent M, Di Carlo I, Rotolo SG, Scaillet B, Burgisser A, et al. 2013. Generation of CO_2-rich melts during basalt magma ascent and degassing. *Contrib. Mineral. Petrol.* 166:545–61
Pleše P, Higgins MD, Mancini L, Lanzafame G, Brun F, et al. 2018. Dynamic observations of vesiculation reveal the role of silicate crystals in bubble nucleation and growth in andesitic magmas. *Lithos* 296–99:532–46
Preuss O, Marxer H, Ulmer S, Wolf J, Nowak M. 2016. Degassing of hydrous trachytic Campi Flegrei and phonolitic Vesuvius melts: experimental limitations and chances to study homogeneous bubble nucleation. *Am. Mineral.* 101:859–75
Proussevitch AA, Mulukutla GK, Sahagian DL. 2011. A new 3D method of measuring bubble size distributions from vesicle fragments preserved on surfaces of volcanic ash particles. *Geosphere* 7:62–69
Proussevitch AA, Sahagian D. 2005. Bubbledrive-1: a numerical model of volcanic eruption mechanisms driven by disequilibrium magma degassing. *J. Volcanol. Geotherm. Res.* 143:89–111
Proussevitch AA, Sahagian DL. 1996. Dynamics of coupled diffusive and decompressive bubble growth in magmatic systems. *J. Geophys. Res.* 101(B8):17447–55
Proussevitch AA, Sahagian DL. 1998. Dynamics and energetics of bubble growth in magmas: analytical formulation and numerical modeling. *J. Geophys. Res.* 103(B8):18223–51
Proussevitch AA, Sahagian DL, Anderson AT. 1993. Dynamics of diffusive bubble growth in magmas: isothermal case. *J. Geophys. Res.* 98(B12):22283–307
Qian M, Ma J. 2009. Heterogeneous nucleation on convex spherical substrate surfaces: a rigorous thermodynamic formulation of Fletcher's classical model and the new perspectives derived. *J. Chem. Phys.* 130:214709
Romano P, Di Carlo I, Adújar J, Rotolo SG. 2021. Water solubility in trachytic and pantelleritic melts: an experimental study. *C. R. Geosci.* 353:315–31
Ryan AG, Russell JK, Nichols ARL, Hess K-U, Porritt LA. 2015. Experiments and models on H_2O retrograde solubility in volcanic systems. *Am. Mineral.* 100:774–86
Sahagian D. 1999. Magma fragmentation in eruptions. *Nature* 402:589–91
Sahagian D. 2005. Volcanic eruption mechanisms: insights from intercomparison of models of conduit processes. *J. Volcanol. Geotherm. Res.* 143:1–16
Sahagian D, Carley TL. 2020. Explosive volcanic eruptions and spinodal decomposition: a different approach to deciphering the tiny bubble paradox. *Geochem. Geophys. Geosyst.* 21:e2019GC008898
Saxena R, Caneba GT. 2002. Studies of spinodal decomposition in a ternary polymer-solvent-nonsolvent system. *Polymer Eng. Sci.* 42:1019–31
Schanofski M, Fanara S, Schmidt BC. 2019. CO_2–H_2O solubility in K-rich phonolitic and leucititic melts. *Contrib. Mineral. Petrol.* 174:52
Schmelzer JWP. 1986. The curvature dependence of surface tension of small droplets. *J. Chem. Soc. Faraday Trans.* 82:1421–28
Schmelzer JWP, Abyzov AS, Baidakov VG. 2019. Entropy and the Tolman parameter in nucleation theory. *Entropy* 21:670
Schmelzer JWP, Gutzow I, Schmelzer J. 1996. Curvature-dependent surface tension and nucleation theory. *J. Coll. Interface Sci.* 178:657–65
Schmelzer JWP, Mahnke R. 1986. General formulae for the curvature dependence of droplets and bubbles. *J. Chem. Soc. Faraday Trans.* 82:1413–20

Shea T. 2017. Bubble nucleation in magmas: a dominantly heterogeneous process? *J. Volcanol. Geotherm. Res.* 343:155–70

Sowerby JR, Keppler H. 2002. The effect of fluorine, boron and excess sodium on the critical curve in the albite–H_2O system. *Contrib. Mineral. Petrol.* 143:32–37

Sparks RSJ. 1978. The dynamics of bubble formation and growth in magmas: a review and analysis. *J. Volcanol. Geotherm. Res.* 3:1–37

Tait S, Jaupart C, Vergniolle S. 1989. Pressure, gas content and eruption periodicity of a shallow, crystallising magma chamber. *Earth Planet. Sci. Lett.* 92:107–23

Tamic N, Behrens H, Holtz F. 2001. The solubility of H_2O and CO_2 in rhyolitic melts in equilibrium with a mixed CO_2–H_2O fluid phase. *Chem. Geol.* 174:333–47

Tolman RC. 1948. Consideration of the Gibbs theory of surface tension. *J. Chem. Phys.* 16:758–74

Tolman RC. 1949. The effect of droplet size on surface tension. *J. Chem. Phys.* 17:333–37

Toramaru A. 1989. Vesiculation process and bubble size distributions in ascending magmas with constant velocities. *J. Geophys. Res.* 94(B12):17523–42

Toramaru A. 2006. BND (bubble number density) decompression rate meter for explosive volcanic eruptions. *J. Volcanol. Geotherm. Res.* 154:303–16

Toramaru A. 2014. On the second nucleation of bubbles in magmas under sudden decompression. *Earth Planet. Sci. Lett.* 404:190–99

Tramontano S, Gualda GAR, Ghiorso MS. 2017. Internal triggering of volcanic eruptions: tracking overpressure regimes for giant magma bodies. *Earth Planet. Sci. Lett.* 472:142–51

Walker D, Mullins O Jr. 1981. Surface tension of natural silicate melts from 1,200°–1,500°C and implications for melt structure. *Contrib. Mineral. Petrol.* 76:455–62

Webster JD, Kinzler RJ, Mathez EA. 1999. Chloride and water solubility in basalt and andesite melts and implication for magmatic degassing. *Geochim. Cosmochim. Acta* 63:729–38

Wedekind J, Chkonia G, Wölk J, Strey R, Reguera D. 2009. Crossover from nucleation to spinodal decomposition in a condensing vapor. *J. Chem. Phys.* 131:114506

Yang N, Li H, Wang G, Wang W, Chen X. 2022. A study of nucleation at initial growth stage of SiC single crystal by physical vapor transport. *J. Crystal Growth* 585:126591

Annual Review of Earth and Planetary Sciences
Volume 51, 2023

Contents

Errata

An online log of corrections to *Annual Review of Earth and Planetary Sciences* articles may be found at http://www.annualreviews.org/errata/earth

Related Articles

From the ***Annual Review of Astronomy and Astrophysics***, Volume 60 (2022)

Atmospheres of Rocky Exoplanets
Robin Wordsworth and Laura Kreidberg

From the ***Annual Review of Chemical and Biomolecular Engineering***, Volume 13 (2022)

Direct Air Capture of CO_2 Using Solvents
Radu Custelcean

Technological Options for Direct Air Capture: A Comparative Process Engineering Review
Xiaowei Wu, Ramanan Krishnamoorti, and Praveen Bollini

From the ***Annual Review of Ecology, Evolution, and Systematics***, Volume 53 (2022)

Evolutionary Ecology of Fire
Jon E. Keeley and Juli G. Pausas

Integrating Fossil Observations Into Phylogenetics Using the Fossilized Birth–Death Model
April M. Wright, David W. Bapst, Joëlle Barido-Sottani, and Rachel C.M. Warnock

The Macroevolutionary History of Bony Fishes: A Paleontological View
Matt Friedman

From the ***Annual Review of Environment and Resources***, Volume 47 (2022)

The Ocean Carbon Cycle
Tim DeVries

Permafrost and Climate Change: Carbon Cycle Feedbacks From the Warming Arctic
Edward A.G. Schuur, Benjamin W. Abbott, Roisin Commane, Jessica Ernakovich, Eugenie Euskirchen, Gustaf Hugelius, Guido Grosse, Miriam Jones, Charlie Koven, Victor Leshyk, David Lawrence, Michael M. Loranty, Marguerite Mauritz, David Olefeldt, Susan Natali, Heidi Rodenhizer, Verity Salmon, Christina Schädel, Jens Strauss, Claire Treat, and Merritt Turetsky

Remote Sensing the Ocean Biosphere
Sam Purkis and Ved Chirayath

From the ***Annual Review of Fluid Mechanics***, Volume 55 (2023)

Submesoscale Dynamics in the Upper Ocean
John R. Taylor and Andrew F. Thompson

Fluid Dynamics of Polar Vortices on Earth, Mars, and Titan
Darryn W. Waugh

Icebergs Melting
Claudia Cenedese and Fiamma Straneo

The Fluid Mechanics of Deep-Sea Mining
Thomas Peacock and Raphael Ouillon

Turbulent Rotating Rayleigh–Bénard Convection
Robert E. Ecke and Olga Shishkina

From the ***Annual Review of Marine Science***, Volume 15 (2023)

From Stamps to Parabolas
S. George Philander

Sociotechnical Considerations About Ocean Carbon Dioxide Removal
Sarah R. Cooley, Sonja Klinsky, David R. Morrow, and Terre Satterfield

Nuclear Reprocessing Tracers Illuminate Flow Features and Connectivity Between the Arctic and Subpolar North Atlantic Oceans
Núria Casacuberta and John N. Smith

The Arctic Ocean's Beaufort Gyre
Mary-Louise Timmermans and John M. Toole

Global Quaternary Carbonate Burial: Proxy- and Model-Based Reconstructions and Persisting Uncertainties
Madison Wood, Christopher T. Hayes, and Adina Paytan

Quantifying the Ocean's Biological Pump and Its Carbon Cycle Impacts on Global Scales
David A. Siegel, Timothy DeVries, Ivona Cetinić, and Kelsey M. Bisson

Novel Insights into Marine Iron Biogeochemistry from Iron Isotopes
Jessica N. Fitzsimmons and Tim M. Conway

Insights from Fossil-Bound Nitrogen Isotopes in Diatoms, Foraminifera, and Corals
Rebecca S. Robinson, Sandi M. Smart, Jonathan D. Cybulski, Kelton W. McMahon, Basia Marcks, and Catherine Nowakowski

Prokaryotic Life in the Deep Ocean's Water Column
Gerhard J. Herndl, Barbara Bayer, Federico Baltar, and Thomas Reinthaler

Lipid Biogeochemistry and Modern Lipidomic Techniques
Bethanie R. Edwards

From the ***Annual Review of Materials Research***, Volume 52 (2022)

Biomineralized Materials for Sustainable and Durable Construction
Danielle N. Beatty, Sarah L. Williams, and Wil V. Srubar III

Brittle Solids: From Physics and Chemistry to Materials Applications
Brian R. Lawn and David B. Marshall

Material Flows and Efficiency
Jonathan M. Cullen and Daniel R. Cooper

Architectural Glass
Sheldon M. Wiederhorn and David R. Clarke